JOC The Journal of Organic Chemistry

Article

pubs.acs.org/joc

Mechanisms of the Reaction between Polyhalogenated Nitrobutadienes and Electron-Deficient Anilines: Computational Modeling

Ozlem Sari,[†,‡] Safiye Sağ Erdem,*[,†] and Dieter E. Kaufmann[§]

[†]Department of Chemistry, Faculty of Arts and Sciences, Marmara University, Goztepe Campus, 34722, Istanbul, Turkey

[‡]Department of Chemistry, Ahi Evran University, 40100, Kırşehir, Turkey

[§]Clausthal University of Technology, Institute of Organic Chemistry, D-38678 Clausthal-Zellerfeld, Germany

Supporting Information

ABSTRACT: Nitro-substituted polyhalogenated butadienes are valuable synthetic precursors for polyfunctionalized bioactive heterocyclic compounds. Recently, a new reaction between 2-nitroperchloro-1,3-butadiene and electron-deficient anilines producing the *Z* stereoisomers of a variety of allylidene arylhydrazines has been reported. Although the formation of a chlorinated nitrile oxide intermediate was proved by trapping it with appropriate alkenes via 1,3-dipolar cycloaddition, the details of the overall mechanism remained unclear. The elucidation of the mechanism is important for a better understanding of polyhalogenated nitrobutadiene chemistry. We proposed six reaction paths for the formation of allylidene arylhydrazine, starting from 2-nitroperchloro-1,3-butadiene and *para*-nitro aniline, and generated the potential energy profiles with the DFT/B3LYP/6-31+G(d,p) method. To include the solvent effect, single-point energy calculations were carried out at the B3LYP/6-31+G(d,p) level by the polarizable continuum model with tetrahydrofuran, as used in the experimental study. The Gibbs activation energies of the rate-determining steps of each mechanism were defined. Taking into account the downhill nature of the overall potential energy profile, Paths 5 and 6 which proceed via extrusion of *p*-nitrophenylisocyanate and the formation of chlorinated nitrile oxide were chosen as plausible mechanisms. Results also provide insights into the chemistry of nitrile oxides, oximes, oxazete, and nitroso compounds as well as S_NVin reactions.

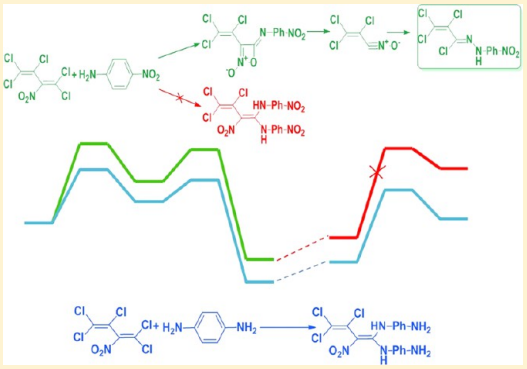

1. INTRODUCTION

Nitro compounds have attracted interest owing to their diverse functionalities. Nitroalkenes are powerful electrophiles; they react with nucleophiles to produce various Michael adducts. They also react as dienophiles in Diels–Alder reactions.[1] Nitro-substituted polyhalogeno-1,3-butadienes are members of a new class of nitroalkenes called polyhalogenated nitrobutadienes, which became the topic of recent investigations because of their interesting chemical and biological properties.[2,3] Generally the choice of building block is 2-nitroperchloro-1,3-butadiene **1a**, which is easily accessible by the introduction of an activating and directing nitro group into 2H-pentachloro-1,3-butadiene.[2a,4]

X-ray analysis indicated that 2-nitroperchloro-1,3-butadiene **1a** and (*Z*)-1,1,4-trichloro-2,4-dinitrobuta-1,3-diene **1b** (Scheme 1) exist in the *s-trans* form in the solid state owing to their bulky substituents.[5]

The experimental studies showed that nitrodiene **1b** acts as a dienophile and reacts with dienes, for example, isoprene, 2,3-dimethylbuta-1,3-diene, cyclopentadiene, or cyclohexa-1,3-diene, in Diels–Alder reactions, whereas perchlorinated nitrodiene **1a** fails regardless of the presence or absence of a Lewis acid. This chemical behavior of **1a** can be rationalized with the steric hindrance caused by five chloro substituents. However, it is well-known that **1a** shows reactivity in vinylic nucleophilic substitution (S_NVin) reactions.[6]

Scheme 1. Nitro-Substituted Polyhalogenobuta-1,3-dienes

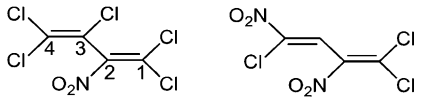

1a **1b**

Analysis of the electron density of the HOMO and LUMO of **1a** by Kaberdin et al.[2a] provides information on the preferred center in the nucleophilic substitution process. It was found that the LUMO of **1a** was located at the activated terminal carbon atom, C-1, of the nitrodichlorovinyl moiety. However, the internal carbon atom, C-3, was also preferred under harsher conditions.[2a,4]

It is well-known that the reaction of **1a** with aromatic amines bearing electron-rich groups leads to the formation of

Received: December 24, 2013
Published: February 17, 2014

   dx.doi.org/10.1021/jo402858j | *J. Org. Chem.* 2014, 79, 2123–2138

Scheme 2. General Reaction of 2-Nitroperchlorobutadiene 1a with 2 equiv of Electron-Deficient Aniline 2 Leading to 3Z

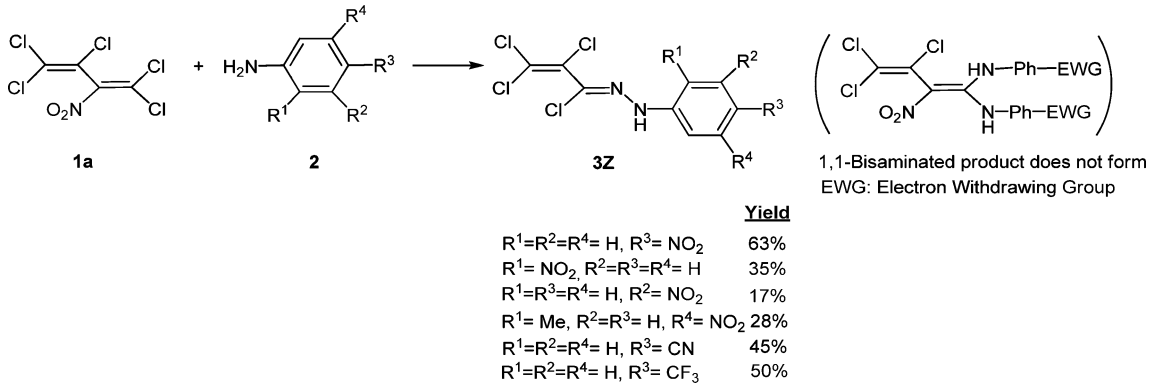

Scheme 3. General Mechanism Proposed

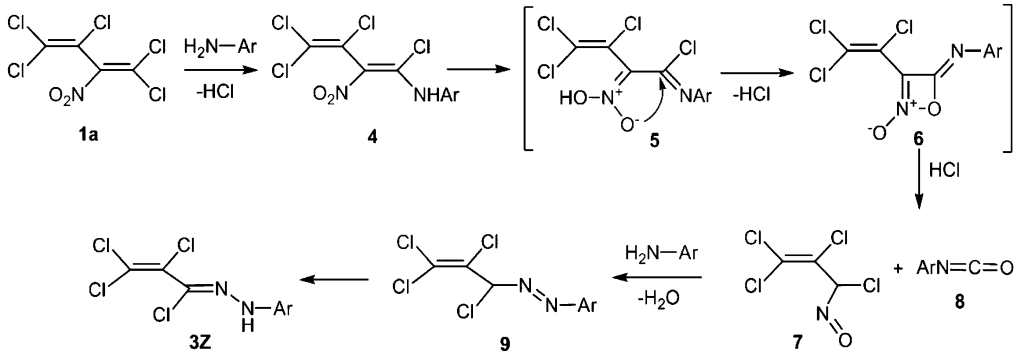

Scheme 4. Formation and Trapping of Chlorinated Nitrile Oxide 11

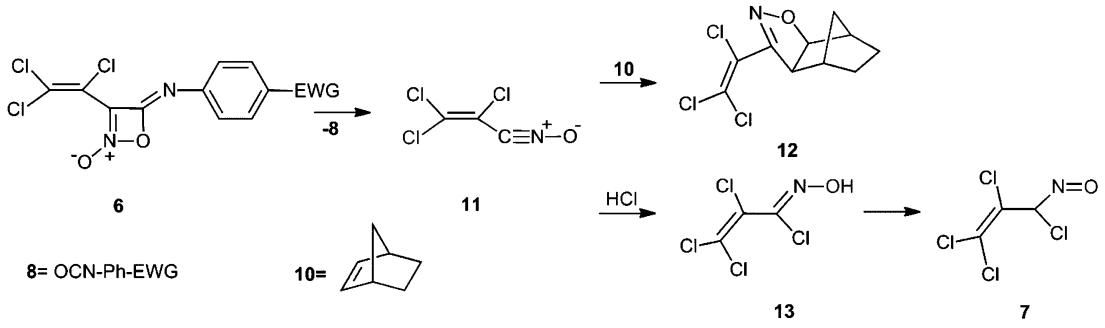

1,1-diamino-2-nitroperchlorobutadienes through the S_NVin pathway.[2a,7] Recently, the reaction between 2-nitroperchlorobutadiene **1a** and 2 equiv of substituted anilines **2** was reported.[2c] Contrary to expectations, with the less basic aniline derivatives having electron-withdrawing groups, the reaction generates *N*-tetrachloro-allylidene-*N*′-arylhydrazines instead of the 1,1-bisaminated substitution product (Scheme 2). Phenylisocyanate is also obtained as the side product. Thus, presumably, a different reaction route was followed after the first vinylic substitution forming allylidene arylhydrazines **3Z**. Interestingly, in addition to IR and NMR spectroscopic investigations, X-ray structural analysis proved that only one single stereoisomer, the *Z* form, was produced. These products should exhibit physiological activity, especially for use in crop science, since aromatic hydrazones show extensive biological activity as fungicidal, fungistatic, antibacterial, or anthelmintic agents.[2c]

It is assumed that the initial step of the reaction is the nucleophilic attack of the deactivated aniline on the positively charged C-1 position of **1a**, followed by tautomerization to imide chloride **5** (Scheme 3). The intramolecular nitronic acid oxygen is more nucleophilic than the amino group of the second molecule of deactivated aniline; it therefore generates cyclic nitrone **6**. Subsequent addition of HCl and cycloreversion of **6** leads to nitroso compound **7** and phenylisocyanate **8**. Addition of a second mol of deactivated aniline and H_2O elimination gives azo compound **9**. Subsequent isomerization leads to the allylidene arylhydrazine derivative **3Z**.[8]

It was assumed that chlorinated nitrile oxide **11** was the precursor of **7** (Scheme 4). To prove the formation of chlorinated nitrile oxide **11**, it was trapped with an alkene via 1,3-dipolar cycloaddition. 1.5 equiv of norbornene **10** was added to the reaction mixture consisting of **1a** and aniline derivative (1.8 equiv) in dry THF to test this hypothesis. Isoxazole **12** was formed in low yield (6%) as proof for the formation of the nitrile oxide intermediate.[8] The other option for the reaction of the chlorinated nitrile oxide is addition of hydrochloric acid to form hydroximoyl **13** that can easily tautomerize to nitroso compound **7**.[8]

dx.doi.org/10.1021/jo402858j | J. Org. Chem. 2014, 79, 2123−2138

Although the formation of the nitrile oxide intermediate is proved by trapping it with an alkene via 1,3-dipolar cycloaddition, the overall mechanism of the reaction between pentachloro-2-nitro-1,3-butadiene **1a** and *p*-nitro aniline **2** remains unclear. The main aim of this study is to employ quantum chemical calculations to clarify the mechanism of the reaction and to present deeper insight into the chemistry of polyhalogenated nitrobutadiene systems. Through this work, additional insights into the chemistry of nitrile oxides, oximes, oxazete, and nitroso compounds as well as S_NVin reactions will also be gained from a broader organic chemistry perspective.

Recently, the annulation reaction of trichloronitroethylene **14** with aniline (Scheme 5) was theoretically modeled by our group.[9] Continuing our computational studies, we hope to present more detailed information about the chemistry of halonitroalkenes and their reactions with aniline derivatives.

Scheme 5. Annulation Reaction of Trichloronitroethylene with Aniline

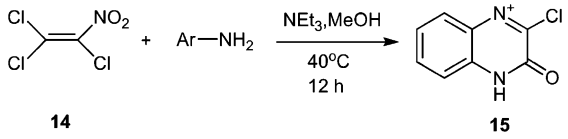

14 **15**

In this paper, we initially proposed six different paths by using density functional theory calculations. All six paths proceed via chlorinated nitroso compound **7**, except Path 3. Path 1 proceeds through *N*-chloronitrone intermediate **18**, whereas Paths 2 and 4−6 include chlorinated nitrile oxide intermediate **11** as the precursor of chlorinated nitroso compound **7**. These six paths have been investigated on the basis of the overall potential energy profiles and the Gibbs free energy barriers of activation of their rate-determining steps.

2. METHODOLOGY

Geometrical parameters of reactants, products, transition states (TSs), and intermediates of all reaction steps were fully optimized with the hybrid density functional B3LYP[10,11] method by using the 6-31+G(d,p) basis set unless otherwise stated, which is known to be reliable for estimating transition-state geometries of a variety of reactions. The B3LYP/6-31+G(d,p) method was chosen as a compromise between accuracy and computational cost based on our previous computational modeling study on the reaction between trichloronitroethylene with aniline.[9] The Gaussian 09[12] program package was used for all calculations. Transition states having an energy maximum in one direction and minima in all others were confirmed by vibrational analysis and characterized by only one imaginary frequency. The intrinsic reaction coordinate[13] (IRC) path was followed to confirm that each transition state connects the corresponding reactant and the product. Thermodynamic calculations were performed at 25 °C and 1 atm. To take into account the solvent effect, single-point energy calculations with the polarizable continuum model[14] (PCM) were carried out at the B3LYP/6-31+G(d,p) level with tetrahydrofuran (THF) as solvent, since this solvent was used in the experimental study. Gibbs free energy corrections calculated for the gas phase stationary points were added to solvation energies to determine free energies of solvation. Thus, the same standard states were taken into account in gas phase and in solvent. Natural bond orbital[15] (NBO) analysis was performed to obtain the charge distribution of some selected stationary points.

3. RESULTS AND DISCUSSION

We formulated six different reaction paths for the formation of allylidene arylhydrazine **3Z** starting from 2-nitroperchloro-1,3-butadiene **1a** and *p*-nitro aniline **2** (Scheme 2). The first five steps leading to the formation of **6** (Scheme 6) are common for all six paths, whereas the last two steps after the formation of **7** (Scheme 7) are common for all paths except Path 3. All the paths investigated are shown in Scheme 7.

3.1. Initial Steps. Potential energy profiles of the initial steps are shown in Figure 1, and each step is discussed below in detail.

*3.1.1. Vinylic Nucleophilic Substitution (S_NVin) Reaction [(**1a**+**2**)→**16**→**4**].* The S_NVin reaction consists of two steps: The first step is the addition of *p*-nitroaniline, and the second step is the elimination of HCl.

In the experimental study, Nutz et al.[8] proposed that the first step of the reaction starts with an S_NVin reaction of **1a** with an aniline bearing an electron-withdrawing group, such as *p*-nitroaniline **2**, to give **16**. During this process, HCl is eliminated from the system. Whether this reaction takes place in a concerted or stepwise manner is an important question. Our attempts to optimize the transition state of the concerted S_NVin reaction failed. Therefore, we propose that this vinylic nucleophilic substitution takes place in two steps. The initial step includes Michael addition, and in the second step, HCl is eliminated from structure **16**, giving S_NVin product **4**. During the Michael addition process, polyhalogenated nitrobutadiene **1a** acts as an electrophile and reacts with *p*-nitroaniline. As we pointed out before, the S_NVin reaction takes place at terminal carbon C1 of **1a**.[2a] The activation energy barrier of the initial step through **TS1**,

Scheme 6. Initial Common Steps of the Reaction of 2-Nitroperchloro-1,3-butadiene with *p*-Nitroaniline

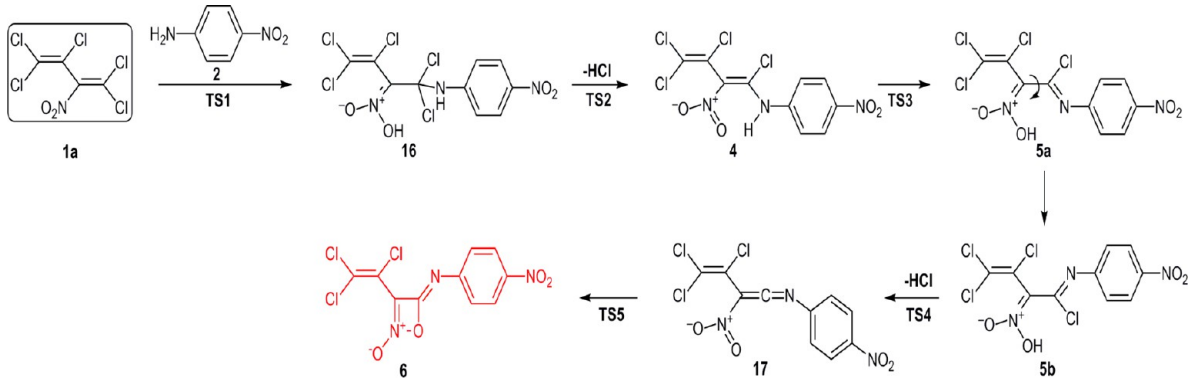

dx.doi.org/10.1021/jo402858j | J. Org. Chem. 2014, 79, 2123−2138

Scheme 7. Paths 1−6 Modeled for the Reaction of 2-Nitroperchloro-1,3-butadiene with *p*-Nitroaniline

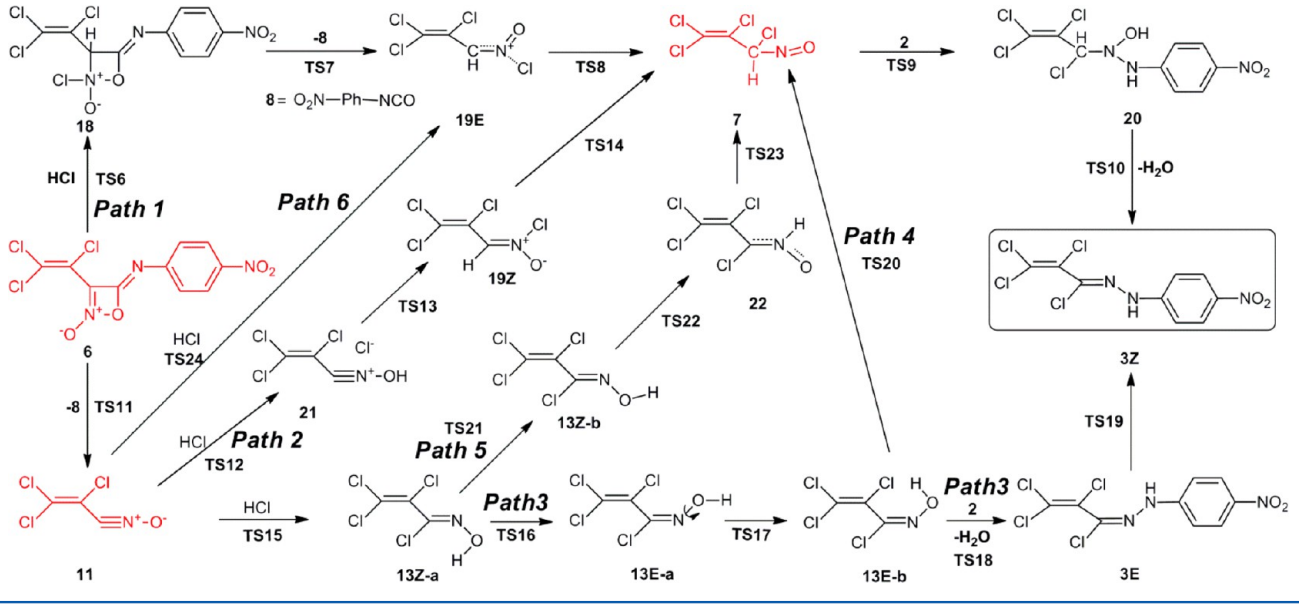

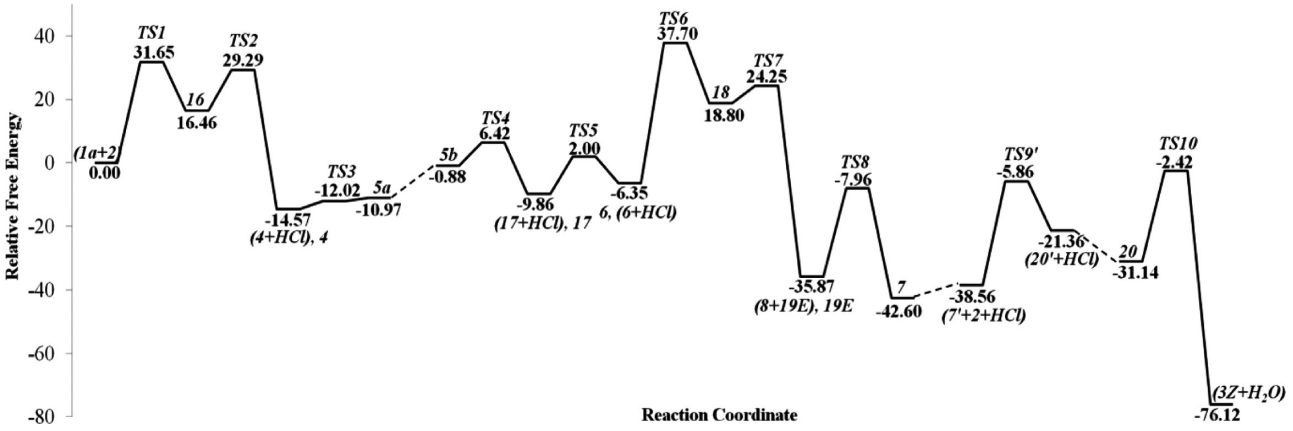

Figure 1. Reaction profile and relative Gibbs free energies (kcal/mol) for the optimized structures in the gas phase related to Path 1.

having only one imaginary frequency of 289.8*i*, is found to be 31.65 kcal/mol in the gas phase (30.59 kcal/mol in THF), and the reaction is endergonic. Reactant complex **RC(1a+2)** is stabilized by intermolecular hydrogen bonding between H14 and O6 with a distance of 2.184 Å, whereas product **16** is stabilized with an intramolecular hydrogen bond between N13 and H14 with a distance of 1.716 Å. While the C1−N13 bond is starting to form, the C1═C2 double bond is converted to a single bond through **TS1** (Figure 2).

Özpınar et al.[9] reported that Michael addition of trichloronitroethylene **14** to aniline exhibits a Gibbs free energy barrier of activation of 27.6 kcal/mol in the gas phase with the same theoretical method that we used. In the present study, the corresponding energy barrier is predicted to be 4 kcal/mol higher, which can be rationalized by the steric hindrance of five bulky chlorine substituents and also the decrease in the nucleophilicity of the aniline because of the *para*-nitro substituent.

The second step of the S_NVin reaction involves elimination of HCl from **16**, which is triggered by the nucleophilic attack of the aniline lone pairs on H14 and proceeds through **TS2**. In **TS2**, while the H15−Cl8 distance decreases to form HCl, H14 migrates to N13 of aniline **2**. It is interesting that N13 abstracts proton H14 and releases proton H15 at the same step. The elimination process is strongly exergonic; it is a facile step with an activation energy barrier of 12.83 and 7.71 kcal/mol in gas phase and in THF, respectively, as shown in Figure 1. A structure similar to that of product **4** was also proposed by Özpınar et al.[9] (Scheme 8) according to results obtained by the same theoretical method used in this study. Additionally, prototype structures **25** and **26** were reported by Lammertsma et al.[16] as shown in Scheme 9.

*3.1.2. 1, 5 Hydrogen Migration (**4**→**5a**).* The conversion of **4** to **5a** proceeds through the 1,5-hydrogen shift of H14 to O6 via fairly flexible six-membered transition-state structure **TS3** (−993.2*i*) having quite a small energy barrier of 2.55 kcal/mol. This small barrier is in agreement with the literature, since it is known that push−pull ethylenes of the same class as nitroenamine derivative **4**, having electron-donor and -acceptor groups at the C═C double bond, exist in equilibrium with nitronic acid derivative **5a**.[17,9] Nitroenamine **4** is 3.6 kcal/mol more stable than nitronic acid **5a**. Bond distance C1−N13 is predicted as 1.344, 1.304, and 1.287 Å in structures **4**, **TS3**, and **5a**, respectively. Intramolecular hydrogen bonds N13−H14···O6 (1.727 Å) in reactant **4** and O6−H14···N13 (1.541 Å) in **5a** stabilize the systems. The C1−C2 distance is 1.389 Å in **4**; it is elongated to 1.426 and 1.445 Å in **TS3** and **5a**, respectively.

dx.doi.org/10.1021/jo402858j | *J. Org. Chem.* 2014, 79, 2123−2138

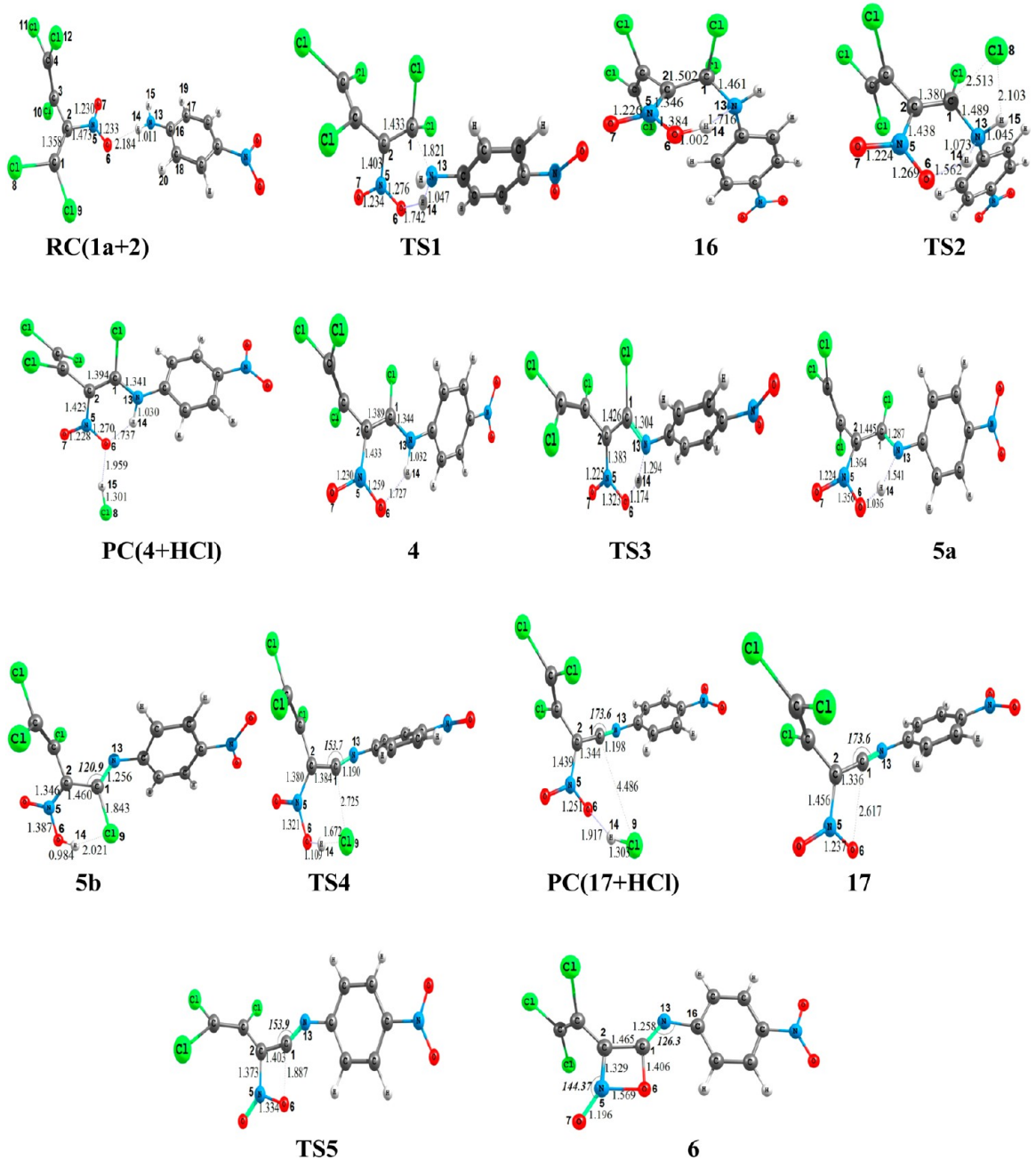

Figure 2. Optimized geometries for the stationary points of the initial steps. Distances are given in angstroms, angles are in degrees.

Scheme 8

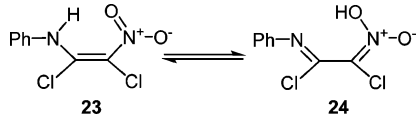

Scheme 9

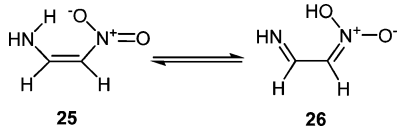

In accordance with our results, similar tautomeric structures nitroenamine **27** and nitronic acid **28** have also been proposed Rajappa et al.[17b] (Scheme 10).

Scheme 10

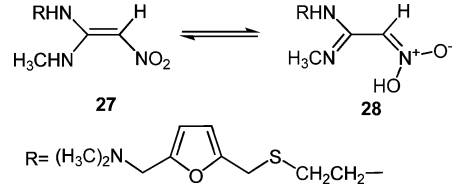

*3.1.3. Conformational Change (**5a→5b**).* Because of electron delocalization, rotation around the C1−C2 bond may be partially restricted. To test this hypothesis, a coordinate-driving potential scan through dihedral angle N13−C1−C2−N5 was performed (Figure S1). Interestingly, it was observed that two different conformational changes, the C−C and N−O bond rotations, were coupled with very small energy barriers.

dx.doi.org/10.1021/jo402858j | J. Org. Chem. 2014, 79, 2123−2138

H14 exhibits intramolecular hydrogen bonding with N13 and Cl9 in **5a** and **5b**, respectively. Hence, the conformational change from **5a** to **5b** is not restricted and occurs spontaneously.

*3.1.4. HCl Elimination [**5b**→(**17**+**HCl**)].* In this step, HCl eliminates from **5b**, passing through **TS4** having only one imaginary frequency of −168.7*i*. IRC calculations have confirmed that this transition state connects reactant **5b** and product complex **PC(17+HCl)**. This step requires a Gibbs free activation energy of 7.30 kcal/mol, which can be easily overcome at room temperature and is found to be exergonic. The C2−C1−N13 bond angle increases from 120.9 to 153.7 and 173.6° for **5b**, **TS4**, and **PC(17+HCl)**, respectively, as a result of the change from the trigonal planar geometry of C1 to linear geometry. Meanwhile, the hybridization of C1 changes from sp^2 to sp. Bond distances C1−Cl9 are found to be 1.843, 2.725, and 4.486 Å in **5b**, **TS4**, and **PC(17+HCl)**, respectively. It should also be noted that an intermolecular hydrogen bond between the HCl hydrogen and the nitro group oxygen (1.917 Å) in **PC(17+HCl)** stabilizes this product complex.

*3.1.5. Formation of Oxazete Intermediate (**17**→**6**).* This step proceeds through **TS5** by the nucleophilic attack of O6 on easily accessible, nearby C1, giving four-membered oxazete ring **6**. This is a facile reaction step having an energy barrier of 11.86 kcal/mol, which is even smaller than the predicted energy barrier (17.9 kcal/mol) of a similar reaction reported by Özpınar et al.[9] for the formation of oxazete derivative **32** shown in Scheme 11 (also at the B3LYP/6-31+G(d,p) level). There

Scheme 11

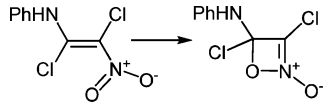

31 **32**

are only a few experimental reports on these interesting ring compounds. Berndt and Wieser[18] reported the formation of the 4H-1,2-oxazete ring, and according to their previous report, this kind of ring seemed to be a reactive intermediate in the thermal and photochemical reactions of *α*,*β*-unsaturated nitro compounds. However, Corkins et al.[19] synthesized a stable 4H-1,2-oxazete derivative with 90% yield, starting from (*Z*)-3,3-dimethyl-1,1-di(methylthio)-2-butanone oxime and *m*-chloroperbenzoic acid in CH_2Cl_2 at 0 °C, as shown in Scheme 12.

Scheme 12

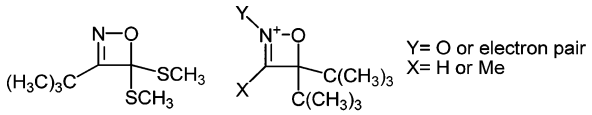

29 **30**

Argilagos et al.[20] proposed an analogous mechanism leading to the formation of oxazete derivative **34** (Scheme 13).

3.2. Path 1. Following the first five common steps described above, Path 1 involves five steps starting with HCl addition to oxazete intermediate **6** as shown in Scheme 7. The potential energy profile is given in Figure 1, and optimized structures are given in Figure 3.

*3.2.1. HCl Addition to the Oxazete Intermediate [(**6**+**HCl**)→**18**].* Addition of HCl to oxazete derivative **6** is a high-energy process with an energy barrier of 44.05 kcal/mol via strained

Scheme 13. Proposal of Argilagos et al.[20]

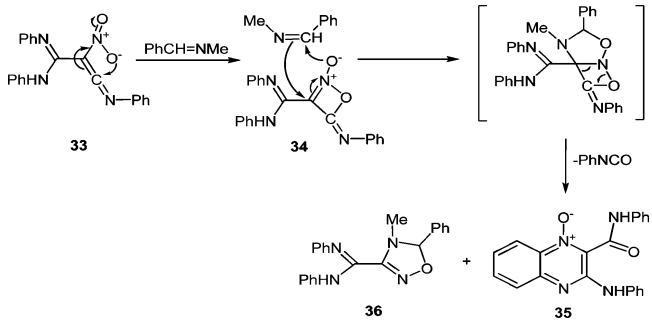

33 **34** **36** **35**

bicyclic **TS6**, and it is endergonic (Figure 1). **TS6** is quite unstable, having 37.70 kcal/mol of energy with respect to the initial reactants. Eventually, this step makes this path an implausible mechanism.

Going from the reactant to the transition-state structure and the product, we can infer that the C3−C2−N5−O7 dihedral angle changes from 3.9° in **RC(6a+HCl)** to 40.3° and −5.6° in **TS6** and **18**, respectively. In product **18**, the N5−Cl22 bond distance is 1.957 Å, which is about 0.2 Å longer than an average nitrogen−chlorine bond distance. This can be rationalized as an ion-pair complex having a positive charge on nitrogen and a negative charge on chlorine. This structure has also been confirmed with NBO analysis (Figure S2). Compound **18** is an unprecedented intermediate that can be characterized as an HCl salt of product **6**. To the best of our knowledge, such an intermediate has not been reported before.

*3.2.2. Cycloreversion [**18**→(**8**+**19E**)].* This process is strongly exergonic. **TS7** is an early transition state, and an extremely low activation energy (5.45 kcal/mol) is required to reach it.

*3.2.3. 1,2-Cl Migration (**19E**→**7**).* This step starts with zwitterionic structure **19E** and leads to product **7**. The reaction is exergonic. It is interesting that Cl migrates from N5 to C2 through a three-membered cyclic structure in **TS8** (Figure 3). An activation energy of 27.91 kcal/mol is needed to reach this transition state.

*3.2.4. Addition of a Second Equivalent of p-Nitroaniline [(**2**+**7**)→**20**].* This step includes the reaction between the second equivalent of deactivated aniline **2** with **7**, giving rise to product **20**, and proceeds via transition state **TS9** having a four-membered strained structure with a high activation energy of 56.34 kcal/mol in the gas phase. However, this energy is reduced considerably when HCl produced from an earlier step is involved in the process. This HCl-assisted step through **TS9′** has a much lower activation barrier of 32.70 kcal/mol in the gas phase as shown on the reaction profile in Figure 1.

*3.2.5. Water Elimination [**20**→(**3Z**+H_2O)].* Water elimination from structure **20** through four-membered cyclic transition state **TS10** leads to allylidene arylhydrazine **3Z**, passing through an activation energy barrier of 28.72 kcal/mol. An intramolecular hydrogen bond is observed between the N5 and H24 atoms in reactant **20**, and the hydrogen-bond distance is estimated to be 1.928 Å. This final step of the reaction is extremely exergonic.

Figure 1 demonstrates that the highest energy barrier of Path 1 with respect to the initial reactants belongs to the HCl addition step occurring through **TS6**. The high barrier (37.70 kcal/mol) of the HCl addition step indicates that Path 1 is not a plausible route for the reaction in consideration.

3.3. Path 2. The first five steps of this path are the same as those discussed in Section 3.1. After the formation of **6**, Path 2

dx.doi.org/10.1021/jo402858j | J. Org. Chem. 2014, 79, 2123−2138

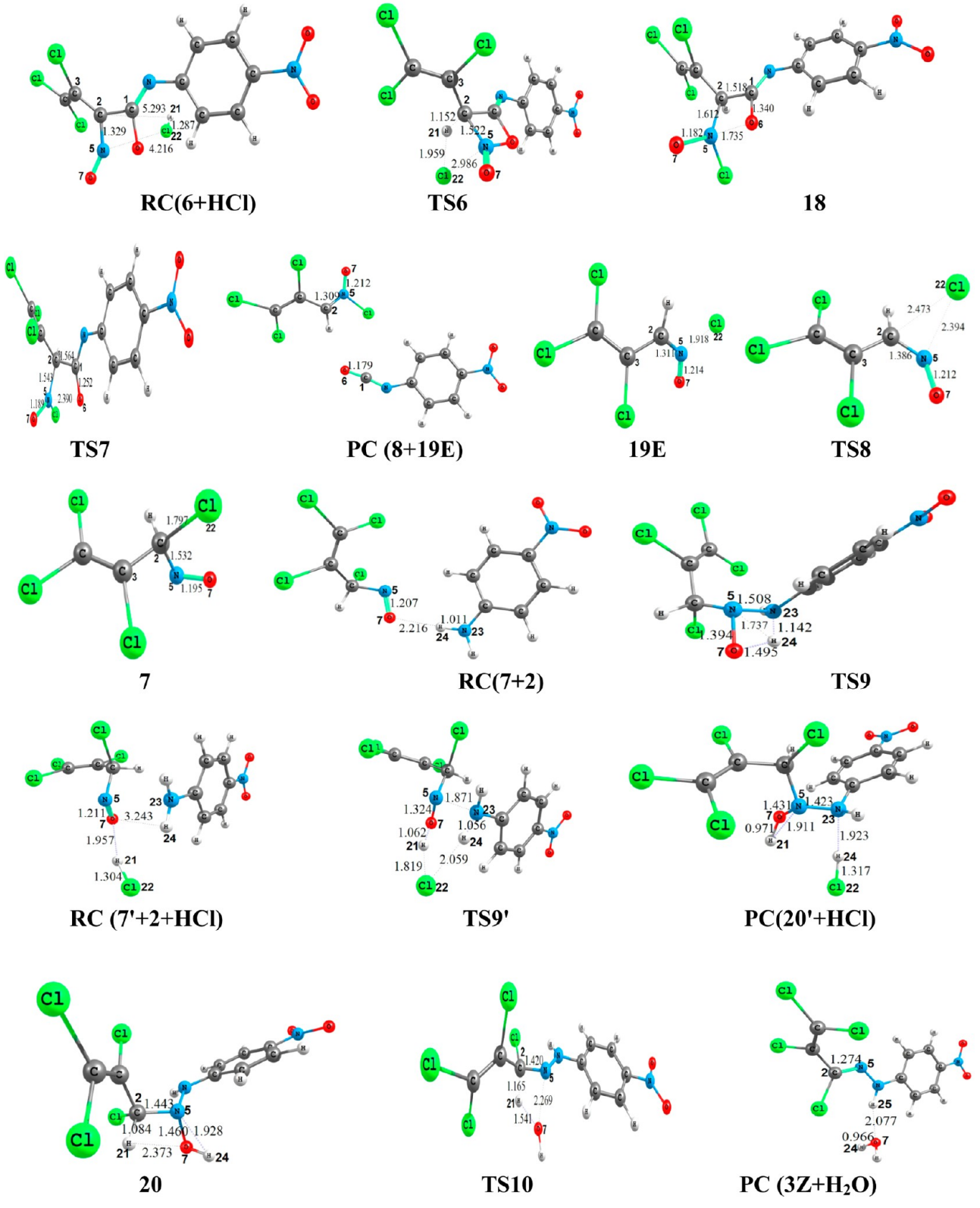

Figure 3. Optimized geometries for the stationary points of Path 1. Distances are given in angstroms, angles are in degrees.

involves six steps leading to the product **3Z**. The potential energy profile is given in Figure 4, and optimized structures related to Path 2 are given in Figure 5.

3.3.1. Extrusion of p-Nitrophenylisocyanate [6→(8+11)]. This step proceeds through **TS11** and generates two products, **8** and **11**, and it is a common initial step for all the paths studied except Path 1. Unfortunately, we were unable to optimize the product complex for this step; however, isolated structures of **8** and **11** were optimized. The energy barrier is found to be 10.23 kcal/mol, and the reaction is quite exergonic.

Extrusion of *p*-nitrophenylisocyanate **8** from oxazete intermediate **6** to generate chlorinated nitrile oxide **11** is a crucial step,

dx.doi.org/10.1021/jo402858j | J. Org. Chem. 2014, 79, 2123−2138

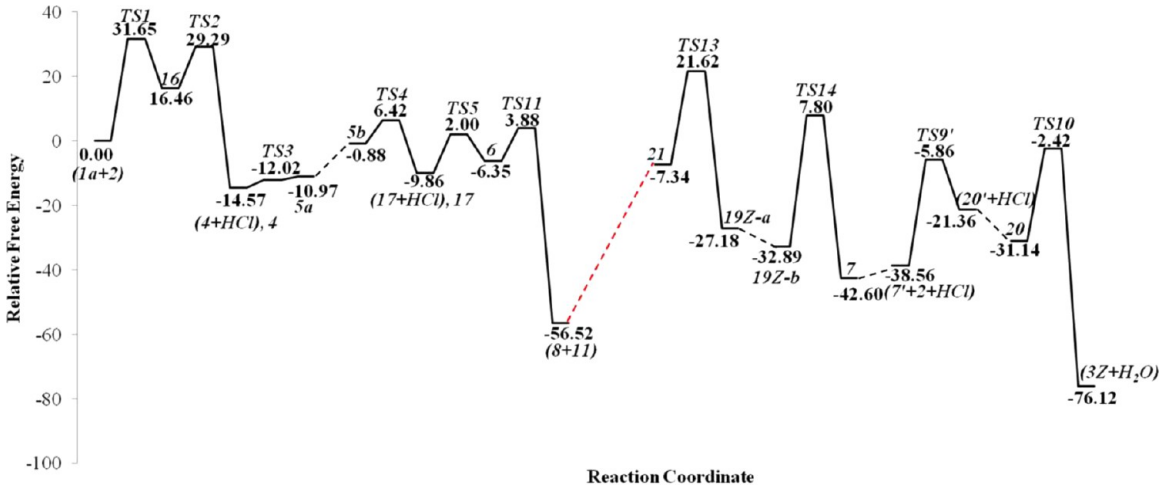

Figure 4. Reaction profile and relative Gibbs free energies (kcal/mol) for the optimized structures in gas phase related to Path 2. **TS12** is not shown since it could only be optimized by PM6.

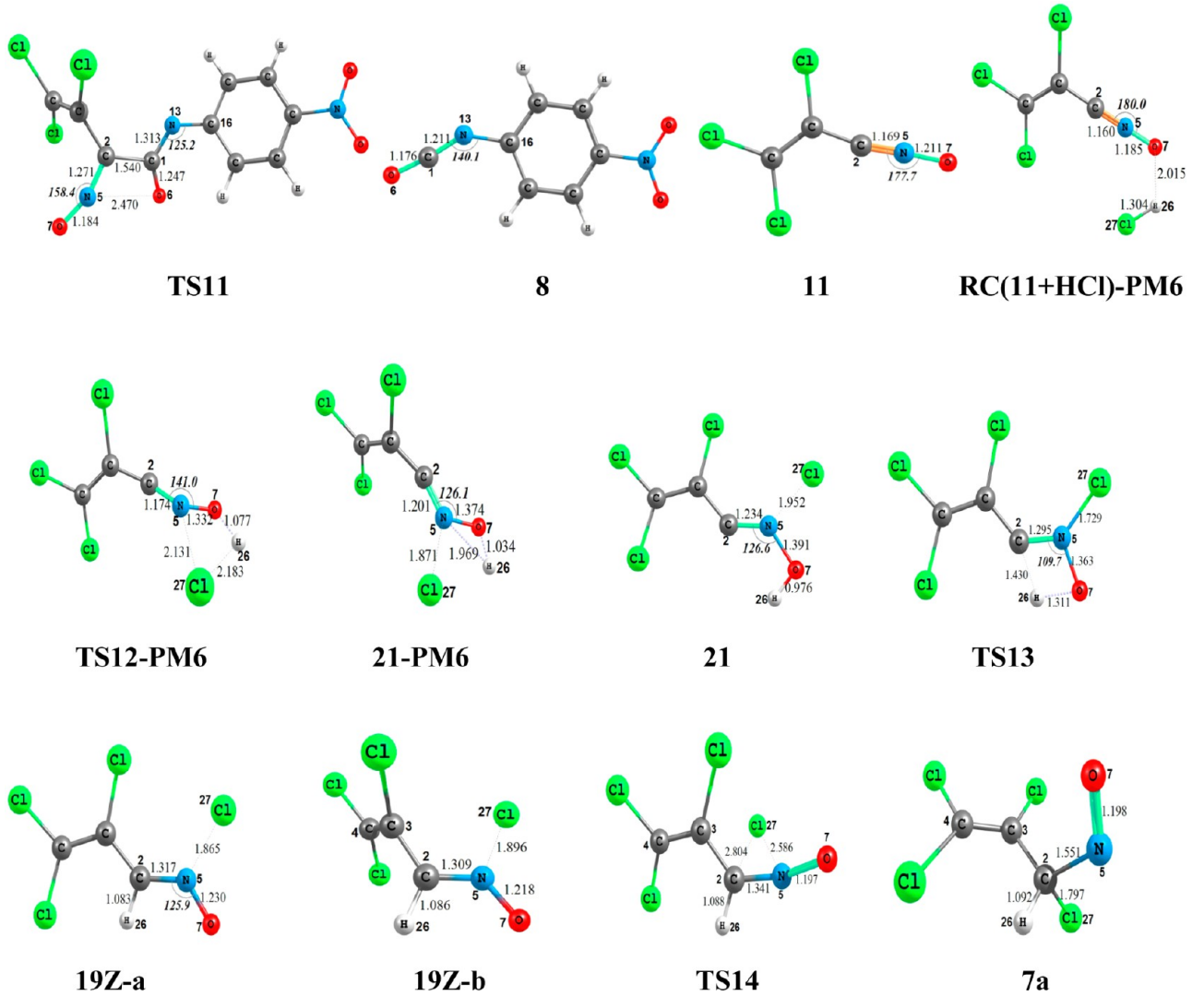

Figure 5. Optimized geometries for the stationary points of Path 2. Distances are given in angstroms, angles are in degrees.

because experimental evidence exists for the formation of both **8** and **11**.[2c,8] Moreover, an analogous extrusion of phenylisocyanate from an oxazete derivative was also reported by Argilagos et al.[20] According to their proposal, oxazete derivative **34** is generated by the nucleophilic attack of oxygen on the C atom of 1,2,4-oxadiazole derivative **33**, a bicyclic intermediate is formed

dx.doi.org/10.1021/jo402858j | J. Org. Chem. 2014, 79, 2123−2138

by 1,3-dipolar cycloaddition with the (benzylidene)(methyl)-amine, and subsequent elimination of phenylisocyanate yields **35** and **36**. They also offer a retro-cycloaddition of the oxazetine *N*-oxide leading to phenylisocyanate and a nitrile oxide, which can undergo 1,3-dipolar cycloaddition with the imine. These proposals are consistent with our modeling study.

3.3.2. Addition of HCl to the Nitrile Oxide Intermediate [(11+HCl)-PM6→21-PM6]. This step of the mechanism could not be optimized with the B3LYP/6-31+G(d,p) method; instead, it was optimized with the semiempirical PM6 method. In order to reach the transition state, 59.98 kcal/mol of activation energy is required. However, the energy of reactant complex **(11+HCl)-PM6** is substantially lower (−56.52 kcal/mol) than that of initial reactants (**1a**+**2**). Therefore, one can assume that the energy evolved in previous steps can be used to overcome the activation energy barrier.

3.3.3. 1,3-Hydrogen Migration (21→19Z-a). In reactant **21**, the three chlorovinyl moieties and C═N(Cl)OH are coplanar and enable conjugation. In order to reach **TS13** from **21**, a Gibbs free energy of activation of 28.96 kcal/mol is required. Solvent THF slightly increases the barrier to 30.02 kcal/mol. Additionally, this step is found to be exergonic.

3.3.4. 1,2-Cl Migration (19Z-b→7a). Prior to this step, **19Z-a** obtained in previous step undergoes a conformational change to its more stable (5.71 kcal/mol) conformer **19Z-b**. Afterward, structure **7a** is formed through the migration of Cl27 starting from **19Z-b** having three possible resonance forms shown in Scheme 14. According to the NBO analysis, forms **19Z-b** and

Scheme 14

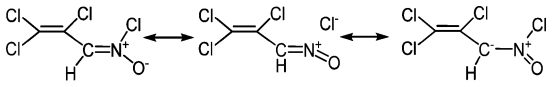

19Z-b **19Z-c** **19Z-d**

19Z-c contribute to the actual structure more than **19Z-d** (Figure S2). This step from **19Z-b** to **7a** needs an activation energy of 40.69 kcal/mol to reach the transition state, and it is also exergonic. The C−N distance is 1.309 Å in **19Z-b**; it increases to 1.341 Å in **TS14** and 1.551 Å in **7a**.

The last two steps of Path 2 are the addition of a second *p*-nitroaniline and water elimination, which are the common steps and have been discussed before for Path 1. However, a conformational change takes place from **7a** to **7** prior to these steps. It is interesting to note that intermediate **19E** formed in Path 1 and **19Z-a** are geometrical diastereomers with respect to the C═N double bond (Scheme 7).

3.4. Path 3. Path 3 starts with the extrusion of **8** from the oxazete intermediate to produce chlorinated nitrile oxide **11**, which has already been discussed in Section 3.3, and continues with HCl addition to nitrile oxide, as shown in Scheme 7. The potential energy profile is given in Figure 6, and optimized structures related to Path 3 are given in Figure 7.

3.4.1. HCl Addition to the Nitrile Oxide Intermediate [(11+HCl)→13Z-a]. As we pointed out before, Nutz et al.[8] indicated that the reaction proceeds from the chlorinated nitrile oxide intermediate, and to prove this hypothesis, they added HCl to the reaction mixture to produce hydroximoyl chloride **13**. Addition of HX to nitrile oxides is well reported.[21] For example, (dimorpholinophosphoryl)nitrile oxide **37** undergoes 1,3-nucleophilic addition reaction with HCl to form the corresponding hydroximoyl chloride **38** (Scheme 15).[21]

Figure 6 shows that addition of HCl to chlorinated nitrile oxide is exergonic and occurs with an activation barrier of 23.51 kcal/mol. While the C2−Cl29 and O7−H28 bonds form, the C2−N5−O7 angle gradually changes from 178.1° in the reactant complex **RC(11+HCl)** to 137.0° and 119.7° in transition state **TS15** and product **13Z-a**, respectively. In transition state **TS15**, the presence of partial double bonds C2−C3 and N5−O7 and a rather long triple bond between C2 and N5 is an indication of electron delocalization that lowers the energy of hydroximoyl chloride **13Z-a**.

3.4.2. cis−trans Isomerization (13Z-a→13E-a). Johnson et al.[22] have reported the hydrolysis of (*Z*)- and (*E*)-*O*-methylbenzohydroximoyl chloride (**39Z** and **39E**) to methylbenzohydroxamates in 1:3 dioxane/water solution. The rate of hydrolysis was found to be quite slow, and the reaction needs relatively high temperatures. Structure **39Z** has been shown to undergo reaction 470 times faster than structure **39E** at 120 °C. This result was rationalized with a stereoelectronic effect. The reaction of **39Z** is faster because of the nonbonding electron pair antiperiplanar to the chloride ion (Scheme 16).[23]

In general, *Z*/*E* isomerization of oximes, which are configurationally stable, does not take place spontaneously, and the rotation around the carbon−nitrogen double bond requires high energy.[24] In parallel to this, the B3LYP/6-31+G(d,p) method predicts an activation energy of 38.75 kcal/mol for the rotation

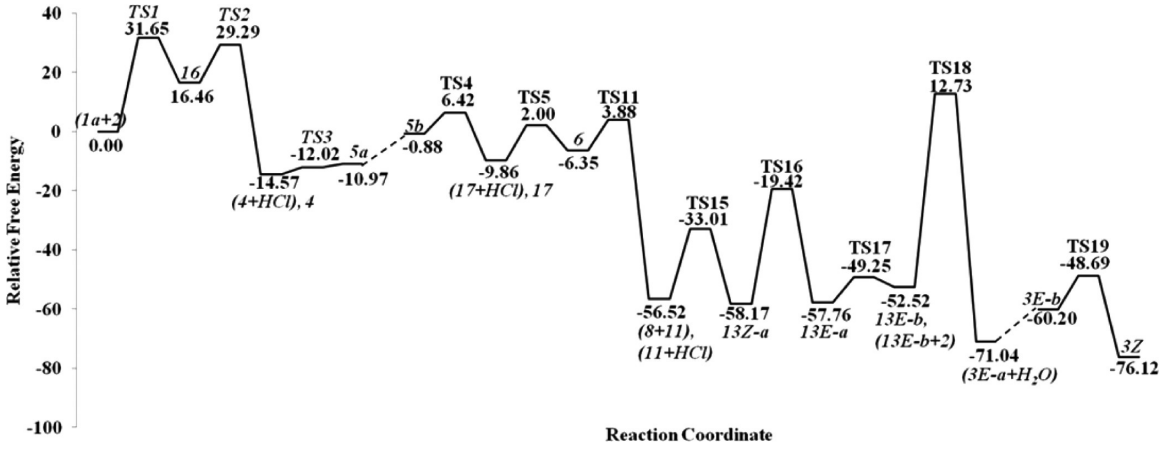

Figure 6. Reaction profile and relative Gibbs free energies (kcal/mol) for the optimized structures in gas phase related to Path 3.

dx.doi.org/10.1021/jo402858j | J. Org. Chem. 2014, 79, 2123−2138

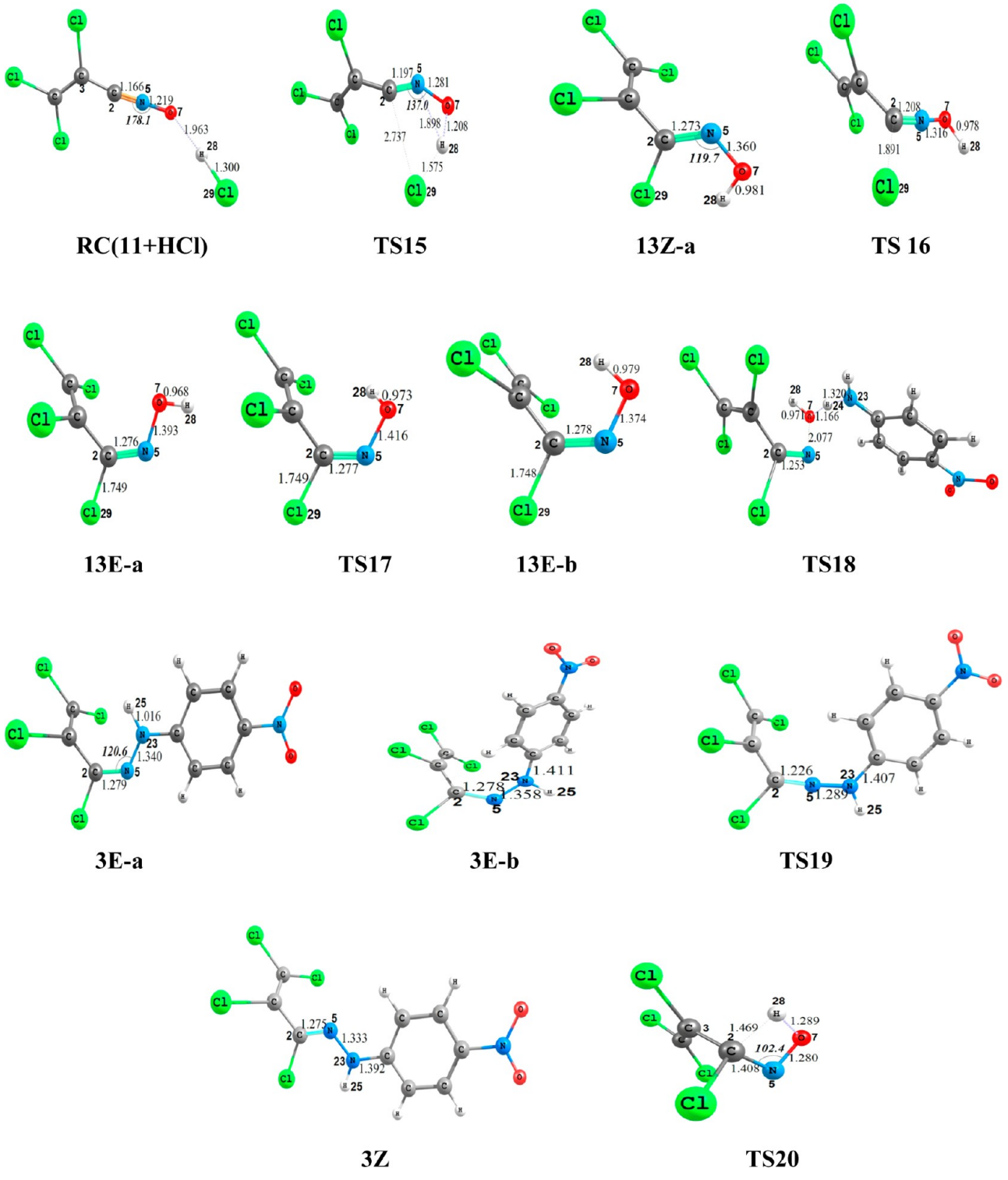

Figure 7. Optimized geometries for the stationary points of Paths 3 and 4. Distances are given in angstroms, angles are in degrees.

Scheme 15. Formation of Oxime Intermediate 38[21]

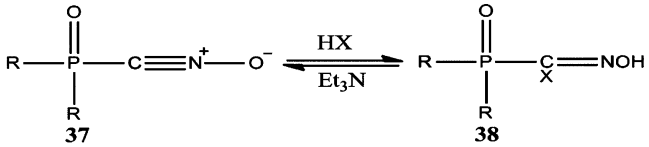

37 **38**

R= morpholino
X=Cl, I

Scheme 16

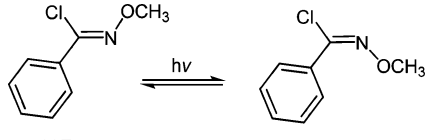

39Z **39E**

dx.doi.org/10.1021/jo402858j | J. Org. Chem. 2014, 79, 2123−2138

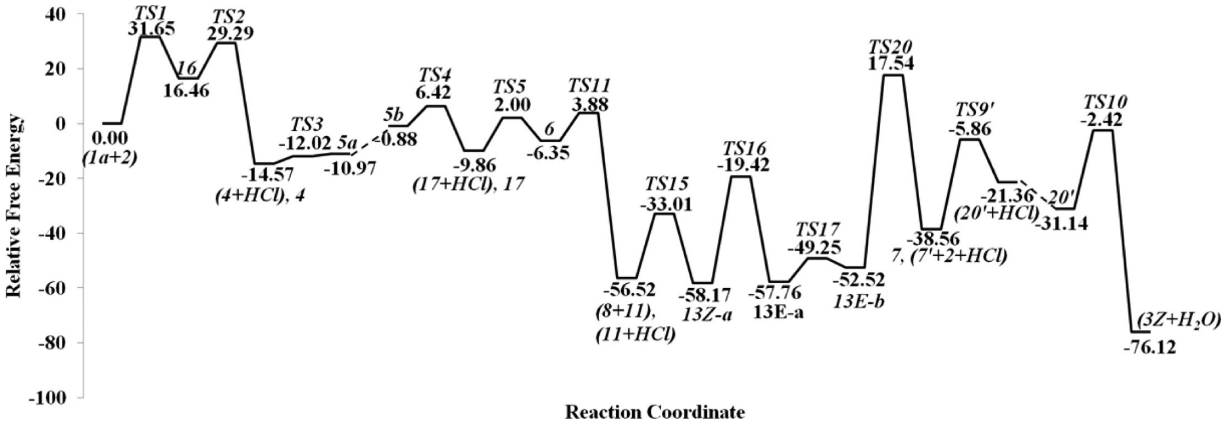

Figure 8. Reaction profile and relative Gibbs free energies (kcal/mol) for the optimized structures in gas phase related to Path 4.

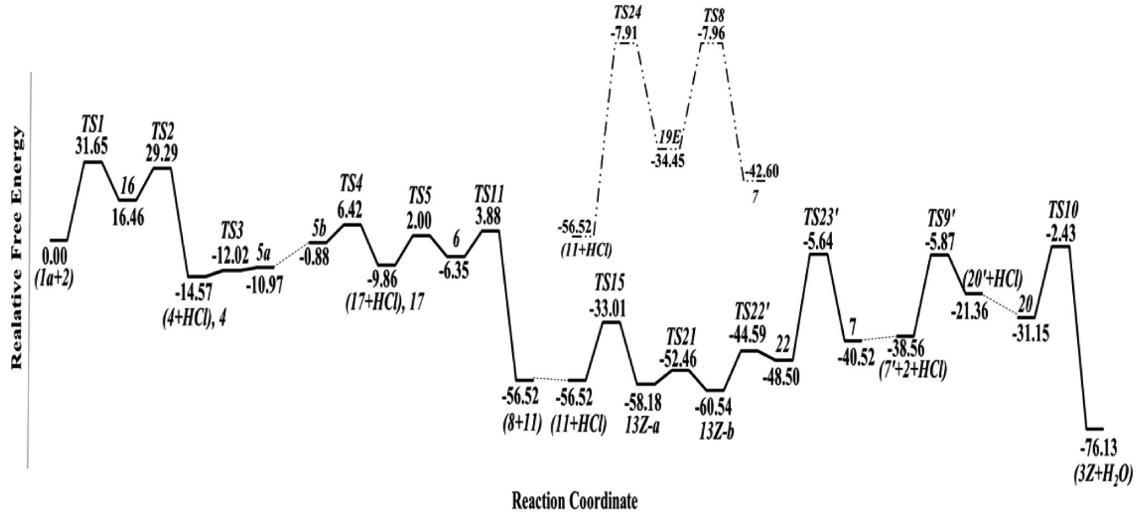

Figure 9. Reaction profile and relative Gibbs free energies (kcal/mol) for the optimized structures in gas phase related to Path 5 (—) and Path 6 (–●●–●●–).

around the carbon–nitrogen double bond in this step. The C2–N5–O7–H28 dihedral angle is −0.7° in reactant **13Z-a**, −154.2° in transition state **TS16**, and 179.7° in product **13E-a**. As it can be observed in Figure 7, there is no conjugation, because of the nonplanarity of the vinyl fragment and the oxime moiety, which results in a relatively high energy barrier.

*3.4.3. Nitrogen–Oxygen Bond Rotation (**13E-a**→**13E-b**).* This step consists of the rotation of the N5–O7 single bond in **13E-a**, leading to product **13E-b** through **TS17**. As expected, this rotational barrier is low, with a Gibbs free energy of 8.52 kcal/mol.

*3.4.4. Addition of a Second Equivalent of p-Nitroaniline to the Oxime [(**13E-b**+**2**)→(**3E-a**+H_2O)].* The reaction of **13E-b** and *p*-nitroaniline **2** leads to allylidene arylhydrazine **3E-a** without producing intermediate **7**. Unfortunately, we were unable to optimize the structures of the product and reactant complexes for this step. Here, while the N–N single bond forms, the N–O bond is broken to eliminate a water molecule from the system, leading to the *E* isomer of the allylidene arylhydrazine, **3E-a**. In order to obtain *Z* isomer **3Z**, an additional step that includes rotation around the C=N double bond is necessary.

As seen in Figure 7, *p*-nitroaniline **2** approaches oxime **13E-b** from the side of the –OH group, which can cause steric hindrance. Unsurprisingly, this step needs an activation energy of 65.25 kcal/mol. Solvent THF increases the barrier to 68.03 kcal/mol, which is quite high, and the reaction is not facile. However, **TS18** lies only 12.73 kcal/mol higher than the initial reactants (**1a**+**2**), and the highly exergonic nature of the reaction coordinate appears to overcome this barrier.

In **3E-a**, the three chlorovinyl moieties and the nitrophenyl moiety are close to each other, which causes steric hindrance. Presumably, **3E-a** (C2–N5–N23–H25, 1.0°) undergoes a conformational change to adopt the structure of the less stable (10.84 kcal/mol) conformer **3E-b** (C2–N5–N23–H25, −167.5°).

*3.4.5. cis–trans Isomerization (**3E-b**→**3Z**).* This step starts with reactant **3E-b** and passes through **TS19** to give final product **3Z**. The *cis–trans* isomerization step is a facile process having a Gibbs free energy of activation of 11.50 kcal/mol, and it is exergonic.

3.5. Path 4. The initial steps of Path 4 are common with those of Path 3 up to the formation of **13E-b**. Afterward, Path 4 proceeds with oxime–nitroso tautomerization (**13E-b**→**7**). The final steps (addition of *p*-nitroaniline and water elimination) are common with those of Paths 1 and 2 and have been discussed before. The potential energy profile is given in Figure 8, and optimized structures related to Path 4 are given in Figure 7.

*3.5.1. Oxime–Nitroso Tautomerization (**13E-b**→**7**).* Generally, in triad systems the keto tautomer is favorable, as the heteroatom prefers π electrons instead of the proton; however,

dx.doi.org/10.1021/jo402858j | J. Org. Chem. 2014, 79, 2123–2138

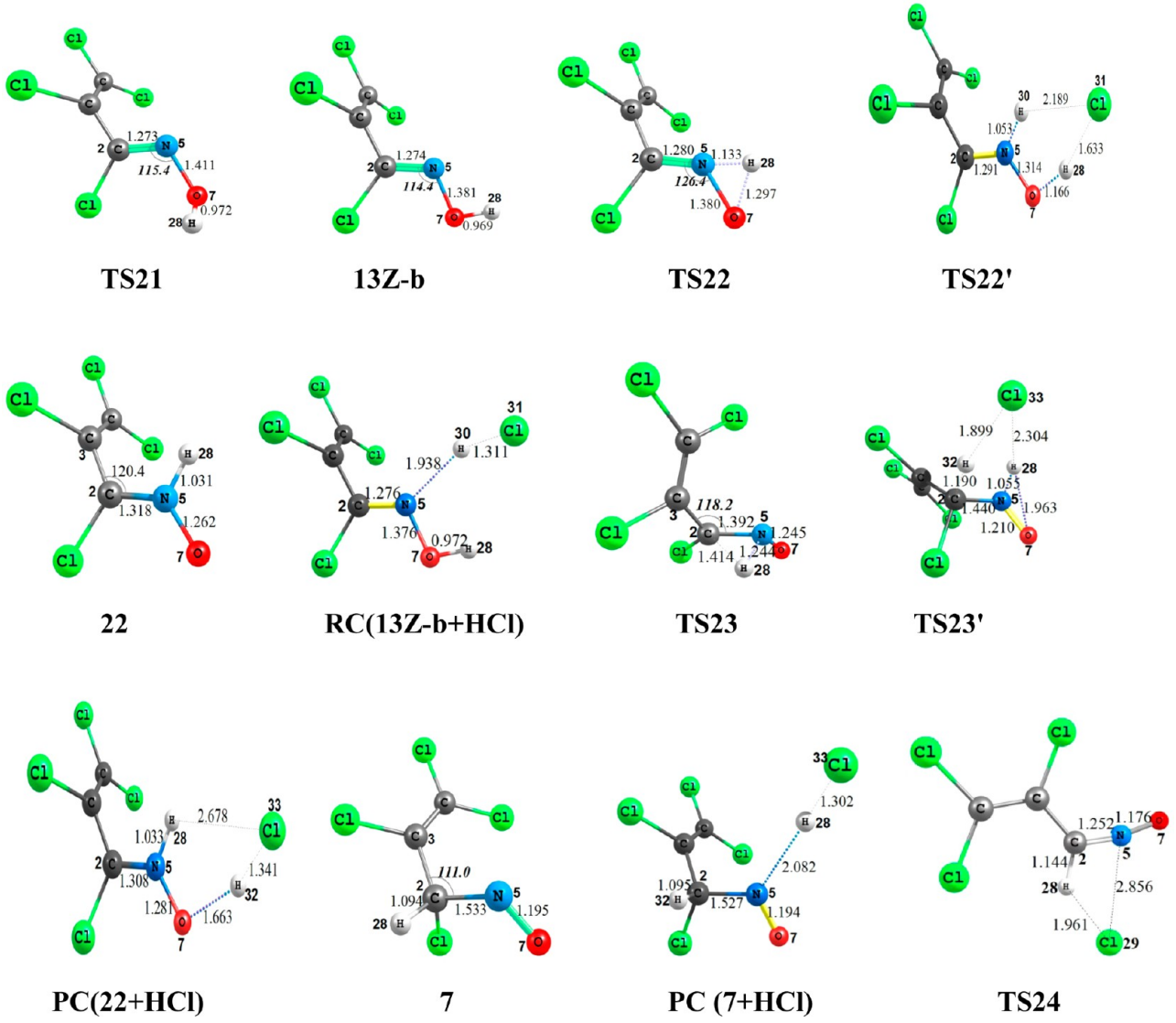

Figure 10. Optimized geometries for the stationary points of Paths 5 and 6. Distances are given in angstroms, angles are in degrees.

in nitroso−oxime tautomeric systems, oxygen prefers the proton instead of π electrons, thus leading to the enol (oxime) tautomer, which is favorable.[25] In parallel to this, we found that oxime tautomer **13E-b** is favored over nitroso tautomer **7** by 13.97 kcal/mol. The calculated barrier for oxime−nitroso tautomerization is 70.05 kcal/mol. The reverse reaction, nitroso−oxime tautomerization, exhibits an activation energy of 56.08 kcal/mol, which is a high barrier as well. Implicit consideration of the solvent did not affect the oxime−nitroso tautomerization barrier substantially. An increase of only 1.81 kcal/mol was observed in THF. However, because of the downhill nature of the potential energy profile, the energy of **TS20** is only 17.54 kcal/mol higher than that of the initial reactants (**1a**+**2**). It appears that the energy evolved from the previous exergonic steps provides most of the energy to overcome this barrier.

3.6. Path 5. The first seven steps of path 5 [(**1a**+**2**)→**13Z-a**] are the same as those discussed for Path 3. In the subsequent reactions, the oxime hydrogen walks from O7 to N5 and then to C2 to give **7** as discussed below. The potential energy profile is given in Figure 9, and optimized structures related to Path 5 are given in Figure 10.

*3.6.1. N5−O7 Bond Rotation (**13Z-a**→**13Z-b**).* The rotation of the N5−O7 bond alters the C2−N5−O7−H28 dihedral angle from −0.8° in **13Z-a** to −82.2° in **TS21** and −180.0° in **13Z-b**. To reach transition-state structure **TS21**, an activation barrier of 5.72 kcal/mol is required. Long et al. used B3LYP/6-311+G(d,p) calculations to study −OH group rotation in a formaldehyde oxime structure.[26] They reported that the *s-trans* form is 5.8 kcal/mol more favorable than the *s-cis* form, as a result of the repulsion between the lone pairs of oxygen and nitrogen. They also reported that this rotation step has an activation barrier of 9.7 kcal/mol, which is considerably higher than the experimental barrier (1.16 kcal/mol). The rotational energy barrier from **13Z-a** to **13Z-b** predicted in this work is between the previously reported values and includes the effect of the vinyl group and the four chloro substituents.

*3.6.2. 1,2-Hydrogen Shift from O7 to N5 (**13Z-b**→**22**).* It is known that the simplest nitrone prefers the formaldoxime tautomer.[27] In order to produce a nitrone tautomer by a 1,2-hydrogen shift, a high activation energy is required. It is interesting to note that the C−N and N−O distances are between those of average C−N and N−O single and double bonds in product **22**, which implies the presence of electron delocalization. This is a

dx.doi.org/10.1021/jo402858j | J. Org. Chem. 2014, 79, 2123−2138

high-energy process with an activation barrier of 52.82 kcal/mol (52.20 kcal/mol in THF) according to B3LYP/6-31+G(d,p) methodology.

Wu and Ho proposed a transition state for 1,2-proton shift from **40Z** to **41Z** using MP2 and G2 methods, and they reported that this process requires an energy barrier of more than 40 kcal/mol (Scheme 17).[28] In our case, the reverse reaction

Scheme 17

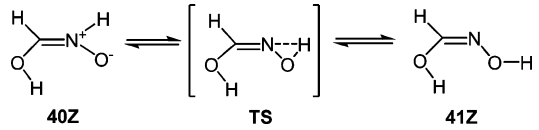

(from **22** to **13Z-b**) corresponds to Scheme 17, and the reverse activation barrier is predicted to be 40.77 kcal/mol, which is in perfect agreement with the MP2 and G2 findings. Interestingly, this high-energy process becomes feasible with HCl-assisted proton transfer passing through **TS22′**. As seen in Figure 9, the HCl-assisted tautomerization reaction occurs with a small activation barrier, 15.95 kcal/mol in the gas phase and 12.75 kcal/mol in THF.

*3.6.3. 1,2-Hydrogen Shift from N5 to C2 (**22**→**7**).* This step involves the transfer of a proton in **22** from N5 to C2, resulting in the formation of nitroso intermediate **7** through **TS23**. The reaction involves stretching of the C2−N5 bond and shortening of the N5−O7 bond. Bond distances and angles are shown in Figure 10. The energy barriers leading to **7** are found to be 47.87 and 48.73 kcal/mol in the gas phase and in THF, respectively.

1,2-Hydrogen shift is also more feasible with the assistance of HCl. With HCl, the activation energy decreased to 42.86 and 42.47 kcal/mol in the gas phase and THF, respectively. Although these barriers are still high, the overall reaction is downhill after **TS1**; **TS23′** is only 5.64 kcal/mol lower in energy than the initial reactants, which indicates that Path 5 is plausible.

3.7. Path 6. Except the channel from **11** to **7**, remaining steps of Path 6 are the same as Path 5. This channel involves the concerted 1,2 addition of HCl to C2−N5 bond of nitrile oxide **11** via **TS24** and gives rise to **19E**. The intrinsic free activation energy to reach **TS24** is 48.61 and 44.40 kcal/mol in gas phase and in THF, respectively. Afterward, **19E** undergoes 1,2-Cl Migration (**19E**→**7**) as discussed in Section 3.2. Although the energy barrier for concerted HCl addition to **11** is high, as in Path5, the overall reaction is downhill after **TS1**; **TS24** and **TS8** are about 8 kcal/mol lower in energy than the initial reactants (**1a**+**2**), which indicates that Path 6 is also plausible. Owing to their similarity, energy profile of Path 6 is shown together with Path 5 in Figure 9. It is noteworthy that, after the formation of (**8**+**11**), all the remaining steps to reach the final product **3Z** exhibit activation barriers below initial reactants. Thus, it appears that exteremly exorgenic nature of (**8**+**11**) production triggers the reaction.

3.8. Formation of Bisaminated Product (*p*-Nitroaniline vs *p*-Aminoaniline). In order to gain a deeper understanding of why aniline derivatives having electron-withdrawing groups generate *N*-tetrachloro allylidene-*N′*-arylhydrazines, instead of 1,1-bisaminated substitution products (Scheme 2), we also modeled the second vinylic substitution on the C-1 atom of perchlorinated nitrodiene **1a** using *p*-nitro- and *p*-aminoanilines. The potential energy profiles (including the first vinylic substitution) are shown in Figure 11, and a 3-D view of the optimized structures is given in Figure 12. The second vinylic substitution of *p*-nitroaniline requires a free energy of activation of 29.62 kcal/mol collectively, which is 16 kcal/mol larger than the corresponding barrier for *p*-aminoaniline and also extremely larger than the energy barriers associated with the steps followed by the formation of **4** (product of first vinylic substitution) in Paths 5 and 6 (Figure 9). Thus, the reaction with *p*-nitroaniline preferentially proceeds through Paths 5 or 6, instead of undergoing a second S_NVin reaction on the C-1 of **1a**.

It is obvious from Figure 11 that the reaction of *p*-aminoaniline exhibits much smaller activation energies and more stable intermediates than the reaction of *p*-nitroaniline. This is in agreement with the experimental observations that electron-rich anilines give 1,1-bisaminated substitution products, whereas electron-poor anilines such as *p*-nitroaniline do not. Calculated NBO charges reveal that the target vinyl carbon of **4-NH$_2$** (0.240) is more electrophilic than that of **4** (0.217) (Figure S2). Moreover, the amino group of **2-NH$_2$** (−0.881) is more nucleophilic than that of **2** (−0.847) as a result of the electron-donating effect of the *p*-NH$_2$ group. These computational results explain the experimental findings.

4. CONCLUSION

Six different reaction paths were proposed in order to understand the details of the mechanism of the reaction between 2-nitroperchloro-1,3-butadiene and *para*-nitro aniline. The potential energy profile of each path was generated relative to the energies of the initial reactants. Comparison of the calculated Gibbs free energies of activation in the gas phase and in THF

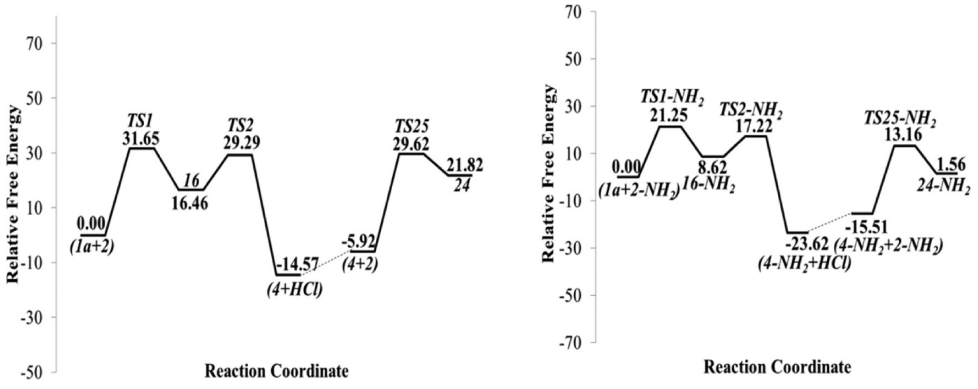

Figure 11. Reaction profile and relative Gibbs free energies (kcal/mol) for the optimized structures in gas phase related to the first and second vinylic substitutions of *p*-NO$_2$-aniline (left) and *p*-NH$_2$-aniline (right).

dx.doi.org/10.1021/jo402858j | J. Org. Chem. 2014, 79, 2123−2138

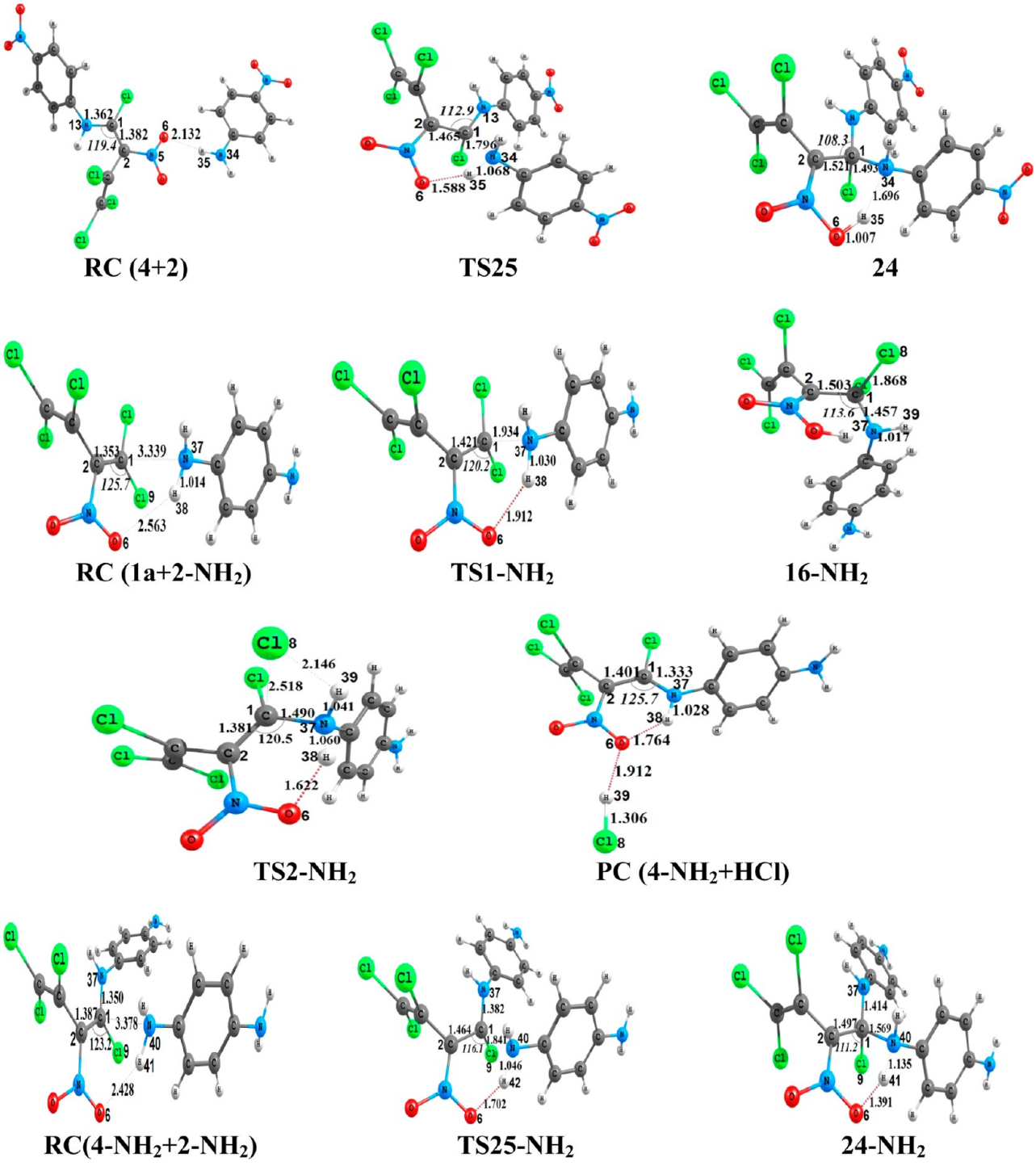

Figure 12. Optimized geometries for the stationary points of the second vinylic substitution. Distances are given in angstroms, angles are in degrees.

revealed that THF did not significantly alter the energetics of the reaction. The results were analyzed in the light of experimental findings to determine the most plausible mechanism.

There are two crucial experimental findings: (1) 1,3-bis(4-nitrophenyl)urea is produced as byproduct (10% yield) together with the main product, **3Z** [*N*-(1,2,3,3,-tetrachloroallylidene)-*N*′-(4-nitrophenyl)hydrazine]. This is strong evidence for the extrusion of *p*-nitrophenylisocyanate **8** during the reaction, because nucleophilic addition of a second mole of *p*-nitroaniline to *p*-nitrophenylisocyanate will produce 1,3-bis(4-nitrophenyl)-urea as byproduct. (2) Chlorinated nitrile oxide **11** is the key intermediate, the existence of which in the reaction channel was proved experimentally by a series of 1,3-dipolar cycloaddition reactions.[8] However, the yield for the intermediate was low (6%),[8] which suggests that alternative routes may be possible.

All proposed paths initially generate oxazete derivative **6**. Five of these paths (Paths 2−6) involve chlorinated nitrile oxide **11**, which is formed by extrusion of **8** from **6**. Path 1 differs from the other five paths in that it does not proceed through chlorinated nitrile oxide **11**, instead a four-membered heterocyclic structure **18** is formed from **6**.

dx.doi.org/10.1021/jo402858j | *J. Org. Chem.* 2014, 79, 2123−2138

For Path 1, HCl addition to oxazete derivative **6** to give **18** is the rate-determining step and exhibits 44.05 and 38.26 kcal/mol of activation energy in the gas phase and in THF, respectively. The corresponding **TS6** is extremely unstable; when the overall reaction profile is considered (Figure 1), the energy of **TS6** is 37.70 kcal/mol higher than that of the initial reactants (**1a**+**2**); therefore, Path 1 is not a plausible mechanism.

For all the other paths studied, the first step of vinylic nucleophilic substitution is the rate-determining step with an activation energy of 31.65 and 30.59 kcal/mol in the gas phase and in THF, respectively. Potential energy profiles of Paths 2−6 (Figures 4, 6, 8, and 9, respectively) are generally downhill with respect to the reactants, **1a** and **2**, and thus they all appear to be plausible. However, for Paths 2−4 there are some pitfalls, which are discussed below.

For Path 2, the transition-state structure of the step involving HCl addition to chlorinated nitrile oxide **11** cannot be optimized with the hybrid density functional B3LYP method using the 6-31+G(d,p) basis set and exhibits a very high energy barrier (59.98 kcal/mol) with the semiempirical PM6 method. Although the previous step is extremely exergonic, the transition-state structure of this step is assumed to be quite unstable. The next step also involves a relatively high-energy transition-state structure, **TS13**. In Path 3, **TS18** is relatively unstable (12.73 kcal/mol higher than initial reactants); therefore, addition of *p*-nitroaniline to oxime derivative **13E-b** to give **3E** requires an activation energy of 65.25 kcal/mol in the gas phase and 68.03 kcal/mol in THF. In Path 4, the energy barrier of the oxime−nitroso tautomerization step is found to be very high, 70.06 and 71.87 kcal/mol in the gas phase and in THF, respectively. The corresponding **TS20** lies 17.54 kcal/mol higher in energy than the initial reactants.

Since the reaction profiles of Paths 5 and 6 are quite similar, we can summarize them together. The highest activation energy (42.47 kcal/mol in THF) in Path 5 belongs to the step involving HCl-assisted 1,2-hydrogen shift from **22** to **7** via **TS23′**. In Path 6, the highest energy barrier is 44.40 kcal/mol in THF which involves concerted addition of HCl to **11** via **TS24**. Although these can be considered as high barriers, they are still much lower than the ones in Paths 2−4. Moreover, the overall reactions are completely downhill after **TS1**; the least stable transition states **TS23′** (in Path 5) and **TS24** (in Path 6) are even lower in energy than the initial reactants (**1a**+**2**). Therefore, our results reveal that Paths 5 and 6 are the two most plausible mechanisms among the paths studied. Both paths are also in agreement with the known experimental findings, in that they proceed via extrusion of *p*-nitrophenylisocyanate **8** and the formation of chlorinated nitrile oxide **11**. After the formation of **8** and **11**, the reaction can follow either alternative path to produce final product **3Z**.

These results elucidate the mechanism of the reaction between *p*-NO_2-aniline and 2-nitroperchloro-1,3-butadiene to give allylidene arylhydrazines. They provide additional mechanistic insight into why anilines with electron-releasing substituent (i.e., *p*-NH_2-aniline) take a different route via second vinylic substitution leading to bisaminated products. In addition, electronic structures and energetics of some nitrile oxides, oximes, oxazete, and nitroso compounds were reported which may guide future studies.

■ ASSOCIATED CONTENT

Supporting Information

Optimized Cartesian coordinates, energies of all stationary points, activation energies in the gas phase and in THF, potential energy scan graph, NBO charges, important geometrical parameters of optimized structures. This material is available free of charge via the Internet at http://pubs.acs.org.

■ AUTHOR INFORMATION

Corresponding Author

*E-mail: erdem@marmara.edu.tr

Notes

The authors declare no competing financial interest.

■ ACKNOWLEDGMENTS

We would like to acknowledge the Marmara University Scientific Research Commission for financial support.

■ REFERENCES

(1) Barrett, A. G. M. *Chem. Soc. Rev.* **1991**, *20*, 95.

(2) (a) Kaberdin, R. V.; Potkin, V. I.; Zapol'skii, V. A. *Russ. Chem. Rev.* **1997**, *66*, 827. (b) Zapol'skii, V. A.; Namyslo, J. C.; Adam, A. E. W.; Kaufmann, D. E. *Heterocycles* **2004**, *63*, 1281. (c) Zapol'skii, V. A.; Nutz, E.; Namyslo, J. C.; Adam, A. E. W.; Kaufmann, D. E. *Synthesis* **2006**, *17*, 2927−2933. (d) Zapol'skii, V. A.; Vogt, E.-J.; Gjikaj, M.; Kaufmann, D. E. *Heterocycles* **2012**, *86*, 1431−1447. (e) Zapol'skii, V. A.; Namyslo, J. C.; de Meijere, A.; Kaufmann, D. E. *Beilstein J. Org. Chem* **2012**, *8*, 621−628. (f) Zapol'skii, V. A.; Fischer, R.; Namyslo, J. C.; Kaufmann, D. E. *Bioorg. Med. Chem.* **2009**, *17*, 4206−4215. (g) Vogt, E. J.; Zapol'skii, V. A.; Nutz, E.; Kaufmann, D. E. *J. Chem. Sci.* **2012**, *67*, 285−294. (h) Zapol'skii, V. A.; Namyslo, J. C.; Gjikaj, M.; Kaufmann, D. E. *J. Chem. Sci.* **2010**, *65*, 843−860. (i) Zapol'skii, V. A.; Yang, X.; Namyslo, J. C.; Gjikaj, M.; Kaufmann, D. E. *Synthesis* **2012**, *44*, 885−894. (j) Zapol'skii, V. A.; Namyslo, J. C.; Gjikaj, M.; Kaufmann, D. E. *Synlett* **2007**, *10*, 1507−1512.

(3) (a) Ibis, C. *Bull. Soc. Chim. Belg.* **1996**, *105*, 317. (b) İbiş, C.; Yıldırım, H. *Phosphorus, Sulfur, and Silicon Relat. Elem.* **2009**, *184*, 369−378. (c) Aydinli, S. G.; Ibis, C. *E-J. Chem.* **2010**, *7*, 1498−1506. (d) Ibis, C.; Tuyun, A. F.; Aydinli, G. *Asian J. Chem.* **2010**, *22*, 1360−1368. (e) Ibiş, C.; Yıldırım, H. *Phosphorus, Sulfur, and Silicon Relat. Elem.* **2011**, *186*, 2236−2249. (f) Deniz, N. H.; Ibis, C. *J. Chem. Sci.* **2013**, *125*, 755−764.

(4) Zapol'skii, V. A.; Namyslo, J. C.; Gjikaj, M.; Kaufmann, D. E. *Arkivoc* **2007**, 76−93.

(5) Potkin, V. I.; Ljakhov, A. S.; Zapol'skii, V. A.; Govorova, A. A.; Kaberdin, R. V. *Dokl. Nats. Akad. Nauk Belarusi* **1996**, *40*, 78.

(6) Zapol'skii, V. A.; Namyslo, J. C.; Blaschkowski, B.; Kaufmann, D. E. *Synlett* **2006**, *20*, 3464−3468.

(7) Ol'dekop, Y. A.; Kaberdin, R. V.; Potkin, V. I.; Shingel, I. A. *J. Org. Chem. USSR (Engl. Transl.)* **1979**, *15*, 39.

(8) Nutz, E.; Zapol'skii, V. A.; Kaufmann, D. E. *Synthesis* **2009**, 2719−2724.

(9) Özpınar, G. A.; Erdem, S. S.; Meyer, C.; Kaufmann, D. E. *J. Org. Chem.* **2009**, *74*, 4727−4739.

(10) Becke, A. D. *J. Chem. Phys.* **1993**, *98*, 5648.

(11) Lee, C.; Yang, W.; Parr, R. G. *Phys. Rev. B* **1988**, *37*, 785.

(12) Frisch, M. J.; Trucks, G. W.; Schlegel, H. B.; Scuseria, G. E.; Robb, M. A.; Cheeseman, J. R.; Scalmani, G.; Barone, V.; Mennucci, B.; Petersson, G. A.; Nakatsuji, H.; Caricato, M.;, Li, X.; Hratchian, H. P.; Izmaylov, A. F.; Bloino, J.; Zheng, G.; Sonnenberg, J. L.; Hada, M.; Ehara, M.; Toyota, K.; Fukuda, R.; Hasegawa, J.; Ishida, M.; Nakajima, T.; Honda, Y.; Kitao, O.; Nakai, H.; Vreven, T.; Montgomery, J. A., Jr.; Peralta, J. E.; Ogliaro, F.; Bearpark, M.; Heyd, J. J.; Brothers, E.; Kudin, K. N.; Staroverov, V. N.; Kobayashi, R.; Normand, J.; Raghavachari, K.; Rendell, A.; Burant, J. C.; Iyengar, S. S.; Tomasi, J.; Cossi, M.; Rega, N.; Millam, J. M.; Klene, M.; Knox, J. E.; Cross, J. B.; Bakken, V.; Adamo, C.; Jaramillo, J.; Gomperts, R.; Stratmann, R. E.; Yazyev, O.; Austin, A. J.; Cammi, R.; Pomelli, C.; Ochterski, J. W.; Martin, R. L.; Morokuma, K.; Zakrzewski, V. G.;. Voth, G. A.; Salvador, P.; Dannenberg, J. J.; Dapprich, S.; Daniels, A. D.; Farkas, Ö.; Foresman, J. B.; Ortiz, J. V.;

Cioslowski, J.; Fox, D. J. *Gaussian 09*, Gaussian, Inc.: Wallingford, CT, 2009.
(13) Gonzalez, C.; Schlegel, H. B. *J. Chem. Phys.* **1989**, *20*, 2514.
(14) Miertus, S.; Scrocco, E.; Tomasi, J. *Chem. Phys.* **1981**, *55*, 117.
(15) (a) Reed, A. E.; Curtiss, L. A.; Weinhold, F. *Chem. Rev.* **1988**, *88*, 889. (b) Foster, J. P.; Weinhold, F. *J. Am. Chem. Soc.* **1980**, *102*, 7211.
(16) Lammertsma, K.; Bharatam, P. V. *J. Org. Chem.* **2000**, *65*, 4662−4670.
(17) (a) Rajappa, S. *Tetrahedron* **1981**, *37*, 1453. (b) Rajappa, S. *Tetrahedron* **1999**, *55*, 7065−7114 and references therein. (c) Nesi, R.; Giomi, D.; Turchi, S. *J. Org. Chem.* **1998**, *63*, 6050.
(18) (a) Wieser, K.; Berndt, A. *Angew. Chem., Int. Ed. Engl.* **1975**, *14*, 69−70. (b) Wieser, K.; Berndt, A. *Angew. Chem., Int. Ed. Engl.* **1975**, *14*, 70−71. (c) Kinstle, T. H.; Stam, J. G. *J. Org. Chem.* **1970**, *35*, 1771. (d) Pinhey, T.; Rizzardo, E. *Tetrahedron Lett.* **1973**, 4057. (e) Sherwood, A. G.; Gunning, H. E. *J. Am. Chem. Soc.* **1963**, *85*, 3506. (f) Surzur, C. M.; Dupuy, C.; Bertrand, M. P.; Nouguier, R. *J. Org. Chem.* **1972**, *37*, 2782.
(19) Corkins, H. G.; Storace, L.; Osgood, E. R. *Tetrahedron Lett.* **1980**, *21*, 2025−2028.
(20) Argilagos, D. M.; Kunz, R. W.; Linden, A.; Heimgartner, H. *Helv. Chim. Acta* **1998**, *81*, 2388−2406.
(21) Belen'kii, L. I. *Nitrile Oxides in Nitrile Oxides, Nitrones, and Nitronates in Organic Synthesis*, 2nd ed.; Feuer, H., Ed.; John Wiley & Sons, Inc.: Hoboken, NJ, 2007 and the references therein.
(22) Johnson, J. E.; Cornell, S. C. *J. Org. Chem.* **1980**, *45*, 4144−4148.
(23) (a) Deslongchamps, P. *Stereoelectronic Effects in Organic Chemistry*; Pergamon Press: New York, 1983. (b) Deslongchamps, P. *Tetrahedron* **1975**, *31*, 2463−2490. (c) Deslongchamps, P. *Heterocycles* **1977**, *7*, 1271−1317.
(24) Bergström, M. A.; Luthman, K.; Karlberg, A.-T. *Chem. Res. Toxicol.* **2007**, *20*, 927−936.
(25) Raczyńska, E. D.; Kosińska, W. *Chem. Rev.* **2005**, *105*, 3561−3612.
(26) Long, J. A.; Harris, N. J.; Lammertsma, K. *J. Org. Chem.* **2001**, *66*, 6762−6767.
(27) Stecko, S.; Paśniczek, K.; Michel, C.; Milet, A.; Pérez, S.; Chmielewski, M. *Tetrahedron: Asymmetry* **2008**, *19*, 1660−1669.
(28) Wu, D.-H.; Ho, J.-J. *J. Phys. Chem. A* **1998**, *102*, 3582.